Organic π-Conjugated Copolymers as Molecular Charge Qubits

C. A. Mujica-Martinez, P. Nalbach, and M. Thorwart

I. Institut für Theoretische Physik, Universität Hamburg, Jungiusstraße 9, 20355 Hamburg, Germany

We propose a design for molecular charge qubits based on π-conjugated block copolymers and determine their electronic structure as well as their vibrational active modes. By tuning the length of the oligomers, the tunnel coupling in the charge qubit and its decoherence properties due to molecular vibrations can be chemically engineered. Coherent oscillations result with quality factors of up to 10^4 at room temperature. In turn, the molecular vibrational spectrum induces strong non-Markovian electronic effects which support the survival of quantum coherence.

PACS numbers: 85.35.−p, 03.65.Yz, 03.67.Lx, 73.22.−f

Nowadays, quantum information is recognized as a physical quantity represented and processed in the form of qubits being governed by the laws of quantum mechanics [1]. Many microscopic systems can be used as qubits [2], but for a successful realization of a quantum computing architecture, a central criterion is a long coherence time, which should be longer than typical gate operation times [3]. Solid-state nanostructures have a high degree of scalability. Spin qubits [4,5] have long coherence times [6,7], but information access is often difficult. Charge qubits [8,9] allow easier coupling to electric fields but, for the same reason, suffer from rapid decoherence.

When growing semiconductor heterostructures, the properties of the charge carriers are controlled via band engineering. The design principles can be transferred to molecular systems to design molecular heterostructures with π-conjugated oligomers [10]. Organic π-conjugated polymers have received great attention since the discovery of their metallic conduction under doping conditions [11]. In their undoped form, conjugated polymers are intrinsically semiconductors which uniquely combine the electronic properties of semiconductors with low cost, versatility of chemical synthesis, ease of processing, and flexibility. Most importantly, their molecular energy scales are much larger than in their inorganic counterparts. Hence, temperature effects are negligible even at room temperature. Organic heterostructures do not suffer from interfacial stress since the heterojunction is a chemical carbon-carbon bond. They can be synthesized by "wet chemistry" [12] and STM polymerization [13] with a spatial precision on the order of 1 nm. Long, highly regular, and well-separated polymer chains are formed. Isolated micrometric polydiacetylene (PDA) chains exhibit quantum spatial coherence limited only by the chain length [14]. Long coherence times have been observed in poly[2-methoxy,5-(2'-ethyl-hexoxy)-1,4-phenylene-vinylene] chains in solution at room temperature [15]. Moreover, individual ladder-type π-conjugated polymers [16] can be addressed spectroscopically and exhibit narrow spectral emission lines, weak interaction with the environment, and rather weak coupling to vibrational modes [17]. A molecular resonant-tunneling diode on the basis of a PDA/ZnPc/PDA molecular nanostructure has been suggested [18] which could operate in air at room temperature and carry negative charges. Moreover, the spectral and electronic properties of π-conjugated copolymers have been shown to be remarkably resilient under structural variations [19]. They can carry Coulombically bound polaron pair spins which show surprisingly long phase coherence times up to several hundreds of nanoseconds at room temperature [20] and can be controlled by electrically detected spin echoes. Clear singlet-triplet spin Rabi oscillations have been reported as well [21].

Here, we propose to design molecular charge qubits from π-conjugated block copolymers. We obtain the electronic energies from quantum chemical calculations and design a molecular double quantum dot (DQD) with energy splittings $\hbar\Delta > k_B T$ at room temperature. Furthermore, we determine the vibrational spectrum, i.e., the infrared (IR) active modes, believed to provide the dominant dephasing channel of the charge qubit. This design can be realized by single π-conjugated molecular heterostructures spanned between a substrate and the tip of an atomic force microscope. This also allows us to address the qubit by voltages with minimal environmental influence. The readout of the charge qubit can be done, e.g., by spectroscopic techniques [22]. We extract a tractable dynamical model and determine the coupling strength between the charge qubit and the IR fluctuations. Varying the length of the oligomers allows us not only to engineer the electronic energies but also the fluctuation spectrum with the possibility to minimize dephasing. To calculate the dissipative dynamics in the presence of strongly non-Markovian IR fluctuations, we use the numerically exact quasiadiabatic path integral. We find rather long coherence times and large quality factors of up to 10^4 at room temperature. We show that they are induced by the strongly non-Markovian electronic dynamics.

Electronic states.—We design π-conjugated block copolymers (see Fig. 1) such that two electronic states
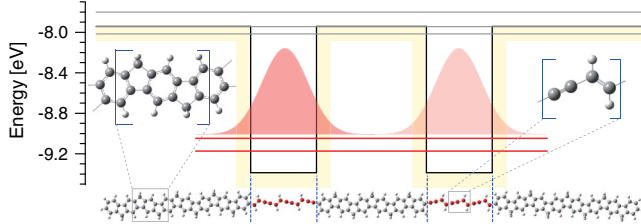
FIG. 1 (color online).   Molecular structure and potential energy profile for electrons within the conduction band for the symmetric DQD l-PPP$_8$/PDA$_3$/l-PPP$_6$/PDA$_3$/l-PPP$_8$. The two energy levels of the confined electronic states are indicated by the horizontal red lines. The wave functions are indicated schematically by the shaded red areas.

are spatially localized in separated regions of the molecule. Undoped organic π-conjugated polymers are intrinsic semiconductors with a band gap $\sim$2 eV. Because of the alignment of the frontier molecular orbitals [10,23], organic heterostructures with three-dimensional confinement of the charge carriers can be constructed to form a DQD. We focus on a combination of ladder-type poly-(p-phenylene) (l-PPP) [16] and PDA since the relatively large offset of 1.4 eV in the conduction band permits design versatility.

To determine the electronic properties, we combine the unrestricted Austin model 1 [24] (AM1) for geometry optimization with the extended Hückel method [25] for single-point electronic-structure calculations with the prefactor $K = 2.43$ for the off-diagonal elements [10,23]. A single unoccupied confined electronic state within the conduction band results from a molecular structure of l-PPP/PDA/l-PPP, thus forming a quantum dot. Two such quantum dots with a short barrier oligomer of l-PPP form a double quantum dot. A charge qubit, with an excess electron localized in the left or right dot, is achieved by doping the molecule single negatively forming a stable polymeric radical anion [26]. Additional molecular cross-tie linkers in the form of methylene bridges avoid twists of the phenyl rings (see Fig. 1).

The resulting double well profile of the conduction band for a DQD structure l-PPP/PDA/l-PPP/PDA/l-PPP is depicted in Fig. 1. The energy splitting $\hbar\Delta$ is the difference between the LUMO and LUMO + 1 energy levels which have been calculated after relaxation of the doped molecular structure. It is controlled by the length of the PDA "well" oligomer and the center "barrier" oligomer l-PPP. Figure 2 shows $\hbar\Delta$ as a function of the well and barrier widths. The width of the lateral barriers is kept large enough to avoid edge effects in the confined energy levels due to the finite size of the molecule. We find energy splittings on the order of hundreds of meV and thus from $\hbar\Delta \sim k_B T$ to $\hbar\Delta \gg k_B T$ at room temperature.

Vibrational states.—Quantum information processing relies on long coherence times of the qubits. The charge qubit in the proposed setup will couple directly to
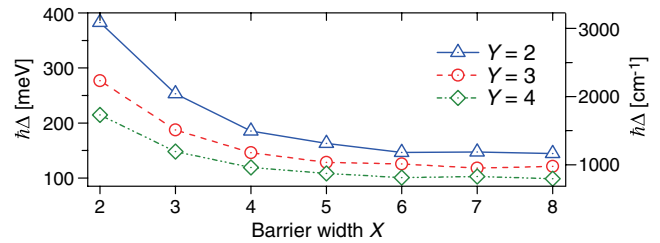
FIG. 2 (color online).   Splitting energy $\hbar\Delta$ as a function of the barrier and well widths for the symmetric DQD l-PPP$_8$/PDA$_Y$/l-PPP$_X$/PDA$_Y$/l-PPP$_8$.

electromagnetic fluctuations and thus also to the active IR excitations of the molecular structure. An example of the IR spectrum for the case $(X, Y) = (3, 2)$ calculated by the AM1 method after including the molecular relaxation due to the single additional electron [27] is shown in Fig. 3. The other cases yield similar spectra (not shown). Roughly, three groups of modes exist: bands with $\nu \sim 1000$ cm^{-1} correspond to vibrations and rotations with twisting and wagging modes outside and scissoring and rocking modes inside the molecular plane; meanwhile, stretching modes for aromatic and aliphatic C-C double bonds are observed around 1500 and 2200 cm^{-1}, respectively. Thus, the splitting energy $\hbar\Delta$ covers the same range of energies as the IR modes (see Figs. 2 and 3). Engineering the molecular structure allows us to choose Δ in relation to the IR spectrum and thus to trim not only the electronic energy splitting of the charge qubit but also its damping behavior. We discuss five molecular heterostructures, which have $N = 0, 1, 2, 3$, and 4 main IR bands at energies below $\hbar\Delta_N$ (see Table I). Next, we determine the coupling between the electronic charge qubit and the IR active modes and establish a tractable model.

Model.—We restrict our considerations of the electronic degrees of freedom to the two states forming the charge qubit (spin effects are neglected), described by a quantum two-level Hamiltonian $H_S = (\hbar/2)(\epsilon\sigma_z - \Delta\sigma_x)$. External
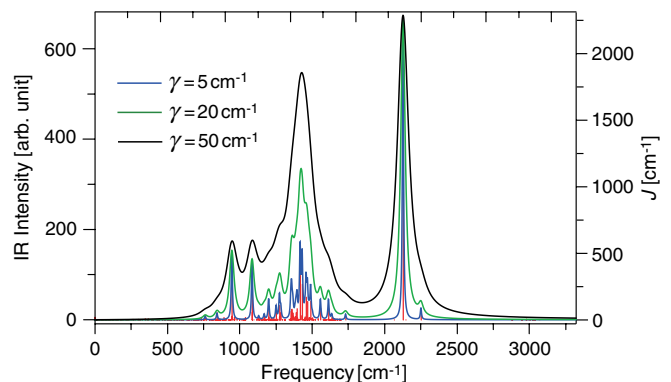
FIG. 3 (color online).   IR spectrum (vertical red lines) of the system l-PPP$_8$/PDA$_2$/l-PPP$_3$/PDA$_2$/l-PPP$_8$. The solid blue, green, and black lines correspond to the spectral density Eq. (2) with $\gamma = 5$, 20, and 50 cm^{-1}, respectively.

TABLE I. Molecular heterostructure l-PPP$_8$/PDA$_Y$/l-PPP$_X$/PDA$_Y$/l-PPP$_8$ whose electronic dynamics is determined by $\hbar\Delta_N$ and influenced by N main vibrational bands.

N	$\hbar\Delta_N$ [meV]	$\hbar\Delta_N$ [cm^{-1}]	(X, Y)	Size [Å]
0	98.8	797.0	(8, 4)	137.6
1	125.7	1014.1	(6, 3)	119.5
2	147.4	1188.8	(7, 2)	113.7
3	253.3	2043.1	(3, 2)	97.2
4	382.7	3086.9	(2, 2)	93.0

electric fields couple to the charge position σ_z, causing an asymmetry ϵ (in general, time dependent). Because of the lacking point symmetry of the molecular structure, small static biases ϵ may arise (increasing with decreasing N). In the following, we neglect this possibility for simplicity (setting $\epsilon = 0$) since we expect only small quantitative changes in the dynamical properties. We are interested in the dynamics of the charge qubit and thus treat its coupling to the IR active modes within an open quantum system approach [28]. Therein, we model all IR modes as harmonic oscillations [29] bilinearly coupled to the charge of the qubit, resulting in a full Hamiltonian

$$H = H_S + \frac{\hbar}{2}\sigma_z\sum_i g_i(a_i + a_i^\dagger) + \sum_i \hbar\omega_i a_i^\dagger a_i \quad (1)$$

with bosonic creation and annihilation operators $a_i^\dagger$ and a_i, oscillator frequency ω_i, and coupling constants g_i.

Finally, we integrate out the bath degrees of freedom, and the influence on the qubit dynamics is fully characterized by the spectral density [28] $J(\omega) = (\pi/2)\sum_i g_i^2\delta(\omega - \omega_i)$. Using the AM1 method, we obtain a structured IR spectrum $\kappa(\omega) = \sum_i I_i\delta(\omega - \omega_i)$ (Fig. 3) with frequencies ω_i and intensities I_i. IR modes couple to the charge of the DQD in the same way as to external electric fields, and accordingly we assume $J(\omega) = \xi \cdot \kappa(\omega)$ with a scaling factor $\xi \sim O(1)$. Thus, $\xi I_i \equiv (\pi/2)g_i^2$. We model each peak in the IR spectrum by a Lorentzian [30,31] with width γ_i. The widths are generated by the coupling of the IR modes to environmental charge fluctuations (from a solvent or substrate) which also generate an Ohmic background spectrum; thus, $J(\omega) \propto \omega$ for small frequencies. In order to maintain the structure of $\kappa(\omega)$ but allow an Ohmic background, we fix $\xi I_i/\omega_i = \tilde{\eta}\eta_i\gamma_i$ with another scaling factor $\tilde{\eta}$. Thereby, we have chosen $\eta_{i_{\max}} = 1$ and $\eta_j = (I_j/I_{i_{\max}})(\omega_{i_{\max}}/\omega_j)$. This leads to the spectral function

$$J(\omega) = \omega\sum_i \frac{\eta_i\gamma_i^2}{(\omega - \omega_i)^2 + \gamma_i^2} = \gamma\omega\sum_i \eta_i L_i(\omega) \quad (2)$$

with Lorentzians $L_i(\omega) = \gamma_i/[(\omega - \omega_i)^2 + \gamma_i^2]$. The ratio $\xi/\tilde{\eta}$ which relates the widths γ_i with the coupling strength of the IR modes to the DQD cannot be determined by our approach. However, the coupling strength can be estimated once the ratio is chosen. Thus, we fix $\xi/\tilde{\eta} = 1$. We also

assume an equal width for all peaks, i.e., $\gamma_i = \gamma$, which then determines also the overall coupling strength between qubit and IR modes. In order to get a tractable analytical expression for the spectral density, only IR modes with an intensity $I_i \gtrsim 0.01I_{i_{\max}}$ are included. Modes with lower intensities are not resolved within the Ohmic background. The final extracted vibrational spectrum is plotted in Fig. 3 for the case $N = 3$.

Electron-vibration coupling.—To calculate the coupling strength between the electronic states and the vibrational modes, we redetermine the energy splittings while the nuclear coordinates are displaced according to the mode with maximal intensity in the IR spectrum. This mode has a maximal electronic coupling strength and should exhibit a maximal shift of the energy splitting. Using AM1, we obtain the eigenvectors of the corresponding mode and displace all atoms accordingly. The largest molecular structure (Δ_0) has its maximal IR mode at $\omega \simeq 2127$ cm$^{-1} = 0.26$ eV with the corresponding force constant $k = 193$ eV/Å^2 as follows from the curvature at the potential minimum. We introduce nuclear displacements corresponding to a potential energy $E_{\text{pot}} = (1/2)k\sum_j \mathbf{r}_j^2 = 8.3$ eV, thereby displacing each atom in its normal mode direction by one unit of the oscillator length and summing over all atoms j. This displaced nuclear configuration is then used to recalculate the electronic states, and we obtain an energy splitting $E^{(\text{dis})} \simeq 2325$ cm^{-1}. Typically, displacements generate an energy difference ϵ_0 for the electron in one of the two wells rather than modifying the tunnel coupling between the two wells. The energy splitting for an according two-level system is then $E^{(\text{dis})} = \sqrt{\Delta_0^2 + \epsilon_0^2}$, whereas in equilibrium $E = \Delta_0$.

The displacements used correspond to the $E_{\text{pot}}/\omega \simeq$ 32nd excited state of the considered mode, leading to $\epsilon_0 \simeq \sqrt{(E^{(\text{dis})})^2 + \Delta_0^2} - \Delta_0 \simeq 926$ cm^{-1}. In turn, a single excitation of this mode corresponds to displacements smaller by a factor $\sqrt{32}$. We assume the electronic qubit states to couple bilinearly to vibrations, i.e., $\propto (1/2)\sigma_z g_j(a_j + a_j^\dagger)$. Hence, all nuclei are maximally displaced relative to a single excitation in the mode ω. This results in an energy difference $\epsilon_0/\sqrt{32}$ which we identify with the coupling constant $g_{i_{\max}}$. Thus,

$$\gamma = (\pi/2)\frac{g_{i_{\max}}^2}{\omega_{i_{\max}}\eta_{i_{\max}}} \simeq 20 \text{ cm}^{-1} \simeq 2.5 \text{ meV}.$$

We note that more elaborate ways to calculate the electronic level widths for different environments are available [32,33]. The structural deformation due to the pseudo-Jahn-Teller effect [34] is negligible since $\gamma \ll \Delta_N$, in contrast to the cases where a strong coherent electron-vibrational coupling leads to qualitative modifications of the electron dynamics [35,36].

Dynamics of the charge qubits.—For all cases here, $\hbar\Delta \gtrsim k_B T$ for $T = 300$ K and thermal effects are negligible. All results reported below are for $T = 300$ K. We study the time-dependent population difference $P(t) = \langle\sigma_z\rangle_t = \text{tr}[\rho(t)\sigma_z]$ of the left and right well. The reduced density matrix $\rho(t)$ is calculated with a quasiadiabatic path integral [37], which is a numerically exact deterministic iteration scheme for nearly arbitrary spectral functions at finite temperatures. We assume an initial preparation $\rho(0)$ in the left well, and the bath is in thermal equilibrium at temperature T. We find very long electronic coherence times as shown in Fig. 4 for all cases. For $\gamma = 20$ cm^{-1}, we obtain decoherence times of $T_{1,N} = 9$, 10, 5, 10, and 24 ps for the configurations $N = 0$, 1, 2, 3, and 4, respectively. These should be compared with the intrinsic oscillation period of 7, 5, 4, 3, and 2 fs, yielding quality factors $Q_N = 1465$, 1919, 1123, 3870, and 14203 for the respective heterostructures. We have investigated electron-vibration coupling strengths up to 250 cm^{-1}. [The $N = 3$ case is shown in Fig. 4(a)]. Coherence times decrease with increasing coupling, but for a fixed γ, the coherence times increase with Δ_N [see Fig. 4(b)]. In turn, the influence of the vibration spectra changes little since the reorganization energy [28] $\lambda = \int_0^\infty d\omega J(\omega)/(\pi\omega) = \gamma\sum_j \eta_j$ differs little between the different cases N. We emphasize that $\hbar\Delta_N$ is not in resonance with any vibrational mode in any of the five cases, which—together with the lacking point symmetry—excludes possible pseudo-Jahn-Teller effects [34]. Put differently, no significant polaron formation occurs. In such a case, the reorganization energy would not be a useful measure for the dephasing influence of the vibrations due to the breakdown of the Franck-Condon approximation. Moreover, due to the spectral overlap around 1500 cm^{-1}, an effective broad single mode is
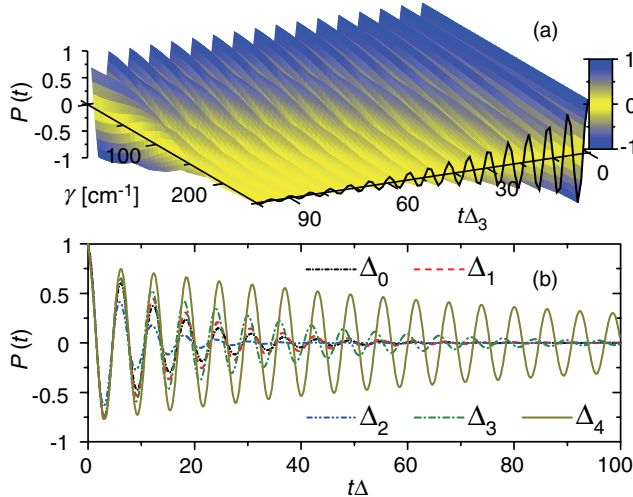
formed. Still, the qubit dynamics is coherent over rather long times. Thus, we conclude that the design of the molecular heterostructure allows us to *chemically* engineer the coherence times. Similar chemical engineering was shown for molecular spin systems [38].

Non-Markovianity.—With increasing Δ_N, the relevant vibrational IR bands shift from $\omega_j > \Delta_0$ to $\omega_j < \Delta_4$. The peaks at frequencies $\omega_j < \Delta_N$ induce strong non-Markovian behavior [39]. Coherent dynamics can be sustained longer by a coherent exchange of energy between the electronic and vibrational degrees of freedom, leading to a dynamical storage of coherence in vibrations which typically have much longer coherence times as compared to electronic degrees of freedom. In order to quantify the non-Markovian effects here, we use a measure [40] based on the trace distance of two quantum states ρ_1 and ρ_2 defined as $D(\rho_1, \rho_2) = (1/2)\,\text{tr}|\rho_1 - \rho_2|$, where $|O| = \sqrt{O^\dagger O}$. It measures the distinguishability of the two quantum states $\rho_{1,2}$, satisfying $0 \le D \le 1$. Under a Markovian evolution, any two initial states become less distinguishable as time increases since information flows only from the system to the environment. Conversely, a dynamical process is defined as non-Markovian if the distinguishability of the pair increases during finite time intervals by backflow of information from the environment to the system. The non-Markovianity

$$\mathcal{N} = \sum_i [D(\rho_1(b_i), \rho_2(b_i)) - D(\rho_1(a_i), \rho_2(a_i))] \quad (3)$$

sums over all time intervals (a_i, b_i) in which D increases. $\mathcal{N}$ may be calculated for finite-dimensional systems only for the few physically relevant initial states [41]. Here, these are $\rho_{1/2}(0)$, being in the left or right well. Figure 5 shows $\mathcal{N}$ for increasing γ. The corresponding trace distances are shown in the inset. We observe an increase of non-Markovian effects for increasing γ until a maximum is

FIG. 4 (color online). Time-dependent population difference $P(t)$ (a) as a function of the damping strengths γ for heterostructure Δ_3 and (b) at fixed $\gamma = 250$ cm^{-1} for all Δ_N with $T = 300$ K. We note that $\Delta_3^{-1} = 2.6$ fs.
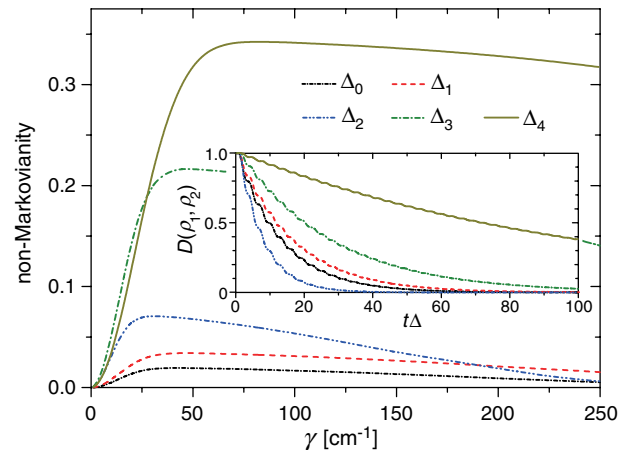
FIG. 5 (color online). Non-Markovianity $\mathcal{N}$ for the five molecular structures as a function of the damping strength. Inset: Time-dependent trace distances for $\gamma = 250$ cm^{-1}.

reached, beyond which $\mathcal{N}$ is decreasing again. The maximum in $\mathcal{N}$ is related with the maximum electron-vibration coupling, which is larger for smaller systems $0 \rightarrow 4$. This shows that non-Markovian behavior can be exploited as a resource of quantum coherence.

Conclusions.—We have proposed a molecular design of electronic charge qubits based on ladder-type poly-(*p*-phenylene) and polydiacetylene π-conjugated polymers, which can serve as the basic elements of a quantum information processor. It can, in principle, operate at room temperature. By tuning the length of the l-PPP and PDA oligomers, the tunneling couplings as well as the dephasing properties can be chemically engineered. Typical quality factors of 10^4 result. Localized vibrational molecular modes induce strong non-Markovian effects, which can help to improve coherence. The experimental verification of these molecular architectures seems feasible by modern technology. Further investigations will elucidate the role of a possible substrate or a solvent.

[1] D. P. DiVincenzo and D. Loss, Superlattices Microstruct. **23**, 419 (1998).

[2] T. D. Ladd, F. Jelezko, R. Laflamme, Y. Nakamura, C. Monroe, and J. L. O'Brien, Nature (London) **464**, 45 (2010).

[3] D. P. DiVincenzo, Fortschr. Phys. **48**, 771 (2000).

[4] D. Loss and D. P. DiVincenzo, Phys. Rev. A **57**, 120 (1998).

[5] B. E. Kane, Nature (London) **393**, 133 (1998).

[6] S. Simmons, R. M. Brown, H. Riemann, N. V. Abrosimov, P. Becker, H.-J. Pohl, M. L. W. Thewalt, K. M. Itoh, and J. J. L. Morton, Nature (London) **470**, 69 (2011).

[7] G. D. Fuchs, G. Burkard, P. V. Klimov, and D. D. Awschalom, Nat. Phys. **7**, 789 (2011).

[8] K. D. Petersson, J. R. Petta, H. Lu, and A. C. Gossard, Phys. Rev. Lett. **105**, 246804 (2010).

[9] D. Harbusch, S. Manus, H. P. Tranitz, W. Wegscheider, and S. Ludwig, Phys. Rev. B **82**, 195310 (2010).

[10] J. C. Arce, A. Perdomo-Ortiz, M. L. Zambrano, and C. A. Mujica-Martinez, J. Chem. Phys. **134**, 104103 (2011).

[11] H. Shirakawa, Angew. Chem., Int. Ed. Engl. **40**, 2574 (2001); A. G. MacDiarmid, *ibid.* **40**, 2581 (2001); A. J. Heeger, *ibid.* **40**, 2591 (2001).

[12] H. Sakaguchi, H. Matsumura, and H. Gong, Nat. Mater. **3**, 551 (2004).

[13] Y. Okawa, M. Akai-Kasaya, Y. Kuwahara, S. K. Mandal, and M. Aono, Nanoscale **4**, 3013 (2012).

[14] F. Dubin, R. Melet, T. Barisien, R. Grousson, L. Legrand, M. Schott, and V. Voliotis, Nat. Phys. **2**, 32 (2006).

[15] E. Collini and G. D. Scholes, Science **323**, 369 (2009).

[16] U. Scherf, J. Mater. Chem. **9**, 1853 (1999).

[17] J. G. Müller, M. Anni, U. Scherf, J. M. Lupton, and J. Feldmann, Phys. Rev. B **70**, 035205 (2004).

[18] Y. Okawa, S. K. Mandal, C. Hu, Y. Tateyama, S. Goedecker, S. Tsukamoto, T. Hasegawa, J. K. Gimzewski, and M. Aono, J. Am. Chem. Soc. **133**, 8227 (2011).

[19] S. Liu, D. Schmitz, S.-S. Jester, N. J. Borys, S. Höger, and J. M. Lupton, J. Phys. Chem. B **117**, 4197 (2013).

[20] W. J. Baker, T. L. Keevers, J. M. Lupton, D. R. McCamey, and C. Boehme, Phys. Rev. Lett. **108**, 267601 (2012).

[21] D. R. McCamey, H. A. Seipel, S.-Y. Paik, M. J. Walter, N. J. Borys, J. M. Lupton, and C. Boehme, Nat. Mater. **7**, 723 (2008).

[22] E. D. Kim, K. Truex, Y. Wu, A. Amo, X. Xu, D. G. Steel, A. S. Bracker, D. Gammon, and L. J. Sham, Appl. Phys. Lett. **97**, 113110 (2010).

[23] C. A. Mujica-Martinez and J. C. Arce, Int. J. Quantum Chem. **110**, 2532 (2010).

[24] M. J. S. Dewar, E. G. Zoebisch, E. F. Healy, and J. J. P. Stewart, J. Am. Chem. Soc. **107**, 3902 (1985).

[25] R. Hoffmann, J. Chem. Phys. **39**, 1397 (1963).

[26] We have performed density functional theory calculations at the B3LYP/6-31G(d) level and found that the total free energy of the radical anion is lower than that of the neutral molecule by about 1 eV.

[27] All calculated frequencies have been multiplied by the scaling factor of 0.954 obtained from the NIST Standard Reference Database 101, Precomputed Vibrational Scaling Factors, http://cccbdb.nist.gov/vibscalejust.asp.

[28] U. Weiss, *Quantum Dissipative Systems* (World Scientific, Singapore, 2008), 3rd ed.

[29] J. L. McHale, *Molecular Spectroscopy* (Prentice-Hall, New York, 1999).

[30] S. Palese, S. Mukamel, R. J. D. Miller, and W. T. Lotshaw, J. Phys. Chem. **100**, 10 380 (1996).

[31] F. Milota, J. Sperling, A. Tortschanoff, V. Szöcs, L. Kuna, and H. F. Kauffmann, J. Lumin. **108**, 205 (2004).

[32] Y. J. Yan and S. Mukamel, J. Chem. Phys. **86**, 6085 (1987).

[33] K. Shan, Y. J. Yan, and S. Mukamel, J. Chem. Phys. **87**, 2021 (1987).

[34] I. B. Bersuker, Chem. Rev. **113**, 1351 (2013).

[35] J. Repp, P. Liljeroth, and G. Meyer, Nat. Phys. **6**, 975 (2010).

[36] F. Reckermann, M. Leijnse, M. R. Wegewijs, and H. Schoeller, Europhys. Lett. **83**, 58 001 (2008).

[37] N. Makri and D. E. Makarov, J. Chem. Phys. **102**, 4600 (1995).

[38] C. J. Wedge, G. A. Timco, E. T. Spielberg, R. E. George, F. Tuna, S. Rigby, E. J. L. McInnes, R. E. P. Winpenny, S. J. Blundell, and A. Ardavan, Phys. Rev. Lett. **108**, 107204 (2012).

[39] M. Thorwart, E. Paladino, and M. Grifoni, Chem. Phys. **296**, 333 (2004).

[40] H.-P. Breuer, E.-M. Laine, and J. Piilo, Phys. Rev. Lett. **103**, 210401 (2009).

[41] H.-S. Zeng, N. Tang, Y.-P. Zheng, and G.-Y. Wang, Phys. Rev. A **84**, 032118 (2011).